

# Highly Conductive Ag/pCF/MVQ Composite Rubber for Efficient Electromagnetic Interference Shielding

Yang Chen<sup>a,b</sup>, Xiao-Ming Shao<sup>a,b</sup>, Liang He<sup>a,b</sup>, Yi-Nuo Xu<sup>c</sup>, Qi-Yuan Yao<sup>a,b</sup>, Ding Feng<sup>a,b</sup>, and Wen-Cai Wang<sup>a,b\*</sup>

<sup>a</sup> State Key Laboratory of Organic-Inorganic Composites, Beijing University of Chemical Technology, Beijing 100029, China

<sup>b</sup> Key Laboratory of Beijing City for Preparation and Processing of Novel Polymer Materials, Beijing University of Chemical Technology, Beijing 100029, China

<sup>c</sup> Sino-german School of Engineering, Qingdao University of Science and Technology, Qingdao 266400, China

**Abstract** In this study, flexible and highly conductive composite rubber at low filler content was successfully prepared through polydopamine-assisted electroless silver plating plus mechanical mixing. Firstly, carbon fibers (CF) were activated by polydopamine (PDA) to improve the surface activity by self-polymerization reaction. Next, because of the metal chelating ability of PDA, silver layer was firmly deposited on the surface of CF through a facile electroless silver plating method. Finally, flexible silver-plated carbon fibers (Ag/pCF) silicone rubber composites prepared by mechanical mixing. By using X-ray photoelectron spectroscopy (XPS) and X-ray diffraction (XRD), the chemical composition and crystal structure of Ag/pCF were examined, and scanning electron microscopy (SEM) was used to assess the surface morphology of the Ag/pCF. The results showed that a uniform and dense silver layer was formed on the surface of the CF, and the conductivity of the Ag/pCF could reach 7885 S/cm. It was noteworthy that the composite rubber filled with only 45 phr Ag/pCF had a high electromagnetic interference shielding effectiveness (100 dB) due to the low density and high aspect ratio of Ag/pCF. The composite rubber has excellent potential for application in the field of electromagnetic interference shielding.

**Keywords** Carbon fibers; Polydopamine; Electroless plating; Silver; Electromagnetic interference shielding

**Citation:** Chen, Y.; Shao, X. M.; He, L.; Xu, Y. N.; Yao, Q. Y.; Feng, D.; Wang, W. C. Highly conductive Ag/pCF/MVQ composite rubber for efficient electromagnetic interference shielding. *Chinese J. Polym. Sci.* 2024, 42, 864–873.

## INTRODUCTION

The increasing complexity of the space electromagnetic environment is causing substantial electromagnetic interference (EMI) due to the widespread use of electronic equipment and the quick development of wireless communication technologies. This not only prevents precision machinery from operating normally but also jeopardizes the health of people.<sup>[1–5]</sup> As a result, it is imperative to prepare high-efficiency EMI shielding materials. Metal materials are widely used due to their excellent conductivity, but they possess disadvantages such as high cost and high density, this limits its application in flexible electronic devices.<sup>[6–9]</sup> Conductive polymer composites (CPCs) are starting to attract a lot of attention due to its many benefits, including changeable electrical conductivity, superior flexibility, and light weight, which has a lot of potential applications in the realm of EMI.<sup>[10–14]</sup> For different application scenarios, EMI shielding materials have formed a series of products, including EMI shielding coatings,<sup>[15]</sup> fabrics,<sup>[16,17]</sup> plastics,<sup>[18,19]</sup> and rubber.<sup>[20–22]</sup> Among these, EMI shielding rubber can be used as an EMI shielding liner to deal with electromagnetic leakage caused by holes or gaps in electronic devices.

Conductive rubber is mainly composed of rubber matrix and conductive fillers, including carbon nanotube,<sup>[23]</sup> graphene oxide,<sup>[24,25]</sup> graphene,<sup>[26]</sup> silver,<sup>[27]</sup> copper,<sup>[28]</sup> and MXene,<sup>[29]</sup> etc. Percolation theory<sup>[30]</sup> suggests that a large number of conductive fillers must be added in order to create the desired conductive network and achieve high conductivity. Hao *et al.*<sup>[31]</sup> prepared silver-plated aluminum microsphere silicone rubber composites, the findings demonstrated that when the content of the conductive filler was 250 phr, the electromagnetic interference shielding effectiveness (EMI SE) of the composites increased to more than 70 dB. Shao *et al.*<sup>[32]</sup> prepared a silver-plated SiO<sub>2</sub> silicone composite rubber with an EMI SE of 90 dB at 300 phr fillers. This leads to an increase in the density, an improvement in its cost and a reduction in its flexibility of the composite rubber. At this time, obtaining high conductivity at low packing fractions is still an important field of research.

Silver-plated carbon fibers (Ag/pCF) with a core-shell structure can solve the problem aforementioned. CF has the advantages of high strength, low density, good mechanical properties, good chemical stability, large aspect ratio, easy to lap each other to form a conductive network. Ag/pCF overcomes the disadvantages of low conductivity of CF<sup>[33–35]</sup> and the shortcomings of high cost and high density of metal. However, the absence of functional groups in active state on the surface of CF and the weak bonding of the plated metal

\* Corresponding author, E-mail: [wangw@buct.edu.cn](mailto:wangw@buct.edu.cn)

Received January 3, 2024; Accepted February 18, 2024; Published online April 3, 2024

to the substrate are easy to fall off, which brings a great challenge to electroless plating.<sup>[36,37]</sup> In order to improve the bonding of CF with silver layer, we chose to deposit a polydopamine layer on the material surface to improve the surface activity. Dopamine (DA) molecules are deposited on the surface of various materials by oxidative self-polymerization in a weakly alkaline aqueous solution at room temperature. Additionally, the PDA molecules are rich in amine and catechol groups, with the latter having the ability to bind with metals,<sup>[38–40]</sup> creating ideal conditions for the subsequent electroless silver-plating process.

Herein, we firstly used dopamine to activate the surface of CF by oxidative self-polymerization of dopamine. Then, with the chelating ability of dopamine on metal ions, the silver layer was firmly deposited on the surface of CF by simple electroless plating. Finally, composite rubber was successfully created by mechanically combining methyl-vinyl silicone (MVQ) and Ag/pCF that had been manufactured. The surface morphology, chemical composition, crystal structure, and EMI shielding effectiveness of this conductive composite rubber were thoroughly investigated. This work provides an idea for realizing highly conductive composites at low filler content.

## EXPERIMENTAL

### Materials

CF with a length of 100–300  $\mu\text{m}$  and a diameter of 7  $\mu\text{m}$  was purchased from Nanjing Weida Composite Material Co., Ltd., China. Dopamine hydrochloride (DA), glucose (GLU), tris(hydroxymethyl)aminomethane (Tris), silver nitrate, potassium sodium tartrate tetrahydrate (PSTT), ammonia, polyvinylpyrrolidone (PVP) and sodium hydroxide (NaOH) were purchased from Shanghai Macklin Biochemical Co., Ltd., China. Triethoxyvinylsilane (A151) and Hydroxy silicone oil was purchased from Beijing Mreda Technology Co., Ltd., China.

### Preparation of PDA Modified CF

DA (0.4 g) and Tris (0.24 g, pH=8.5) were added to 200 mL of distilled water to prepare dopamine modified solution. Next, CF (1.2 g) was immersed and stirred vigorously for 8 h at 25  $^{\circ}\text{C}$ . The products were represented with pCF.

### Electroless Silver Plating on the Surface of pCF

First, NaOH (1.7 g/L), PVP (2.5 g/L), and the appropriate amount of glucose (GLU) or potassium sodium tartrate tetrahydrate (PSTT) were added to the appropriate amount of distilled water to prepare Reducing Solution B. Then  $\text{AgNO}_3$  (7.73 g/L) and the appropriate amount of ammonia were added to the distilled water to prepare Solution A. Added the pCF to solution A and

then slowly added solution B to solution A for electroless silver plating. Next, the product was washed with distilled water and dried in an oven. In order to obtain higher conductivity, the above Ag/pCF was subjected to appropriate heat treatment in a muffle furnace under nitrogen followed by a natural annealing process.

### Salt Spray Corrosion Simulation of Ag/pCF

According to GJB 150.11A-2009, salt spray corrosion simulation experiments were conducted. Add NaCl (20 g) to deionized water (180 mL), add  $\text{H}_2\text{O}_2$  (200  $\mu\text{L}$ ) to simulate the actual working conditions of oxygen, add Ag/pCF (5 g) to the corrosion solution, stirring for 30 min at 35  $^{\circ}\text{C}$ . After repeated rinsing of the corroded fibers with deionized water, they were dried in an oven at 60  $^{\circ}\text{C}$ .

### Preparation of Silicone Rubber Composites

The Ag/pCF was mixed with silicone rubber (100 g), hydroxyl silicone oil (2 g), coupling agent A151 (2 g), fumed silica (15 g), and vulcanizing agent DPBMH (2 g) in Hacker compactor. The mixture was vulcanized at 175  $^{\circ}\text{C}$  for 15 min to obtain conductive composites. The prepared composite rubbers were denoted as Ag/pCF-X/MVQ, where X represented the filler content. The entire preparation process of Ag/pCF/MVQ is shown in Fig. 1.

### Characterization

X-ray photoelectron spectroscopy (XPS, ESCALAB 250 XPS system, Thermo Electron Corporation, USA) was utilized to analyze the chemical state. X-ray diffraction (XRD, XRD-6000, Shimadzu, Japan) was used to characterize the crystal structure of Ag/pCF. Scanning electron microscopy (SEM, Hitachi S-4800, Japan) was used to capture the micro-morphology images. Four-point probe (RTS-8, Guangzhou, China) was used to measure the conductivity of Ag/pCF. Vector network analyzer (VNA, E5071C, USA) was used to test the EMI SE of the shielded composites. Electronic universal testing machine (SANS EMT2000-B, Shenzhen, China) was used to test the mechanical properties of composite rubber.

## RESULTS AND DISCUSSION

### Surface Activation of CF by PDA

Low surface activity limited the application of CF in many applications, CF showed surface inertness due to the lack of reactive groups on the surface, thus CF was modified using polydopamine under weakly alkaline (pH=8.5) conditions to improve surface activity. The C element of pure CF in the C 1s core-level spectra was primarily present as C—C, with a minor quantity of C—O and O—C=O owing to surface oxidation, as illus-

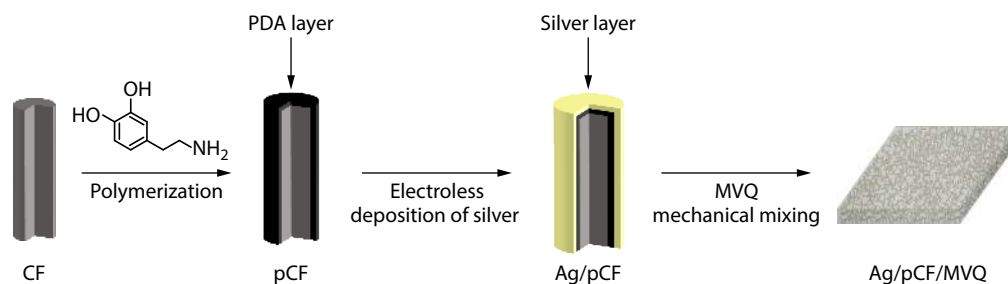


Fig. 1 Process for the preparation of conductive Ag/pCF/MVQ.

trated in Figs. 2(a). After the surface functionalization with PDA, the intensity of the C—O peaks (286.6 eV) and the O—C=O peaks (288.5 eV) of pCF were significantly enhanced, and the main peak in the vicinity of 284.6 eV of pCF was obviously broadened (Fig 2c). This was due to the fact that the PDA layer contains a large number of C—N bonds, resulting in a new strong peak at 285.5 eV. Similarly, as shown in Fig 2(d), the N 1s core-level spectra of pCF shows two new fitted peaks with a BE of 399.5 eV for the —N—H bond and a binding energy of 398.5 eV for the —N=. [41] The appearance of the —N—H bond was attributed to the backbone of the dopamine, and the —N= was attributed to the formation of an indole moiety in the process of oxidative self-polymerization of the dopamine. The results indicated that after a simple reaction, dopamine was effectively coated on the CF surface.

### Preparation of Ag/pCF

Thanks to the possession of a large number of reactive groups, including catechol groups and quinone groups, PDA could chelate silver ions and reduce small amounts of silver ions to silver nanoparticles (AgNPs). These AgNPs could provide nucleation sites for silver growth during the chemical plating process and formed a uniform and robust silver layer after the addition of a reducing agent. Fig. 3(a) shows the XPS broad scan spectra of Ag/pCF after electroless silver plating shows distinct peaks characteristic of the Ag 3p and Ag 3d orbitals. The Ag 3d spectra show the two peak components, with a binding energy of 368.2 eV for the Ag 3d<sub>5/2</sub> substance and 374.2 eV for the Ag 3d<sub>3/2</sub>

substance (Fig 3b), which were attributed to the Ag<sup>0</sup> substance. Besides, the XRD pattern of Ag/pCF (Fig. 3c) shows strong silver diffraction peaks. The 2 $\theta$  values of the five diffraction peaks of silver are 38.2°, 44.4°, 64.6°, 77.4° and 81.6°, corresponding to the (1 1 1), (2 0 0), (2 2 0) and (3 1 1) faces and the (2 2 2) face of face-centred cubic silver, respectively (JCPDS 04-0783). [42] No diffraction peaks of silver halides or silver oxides were observed, indicating that the silver layer on the CF surface was of high purity.

To investigate the effect of the quality of surface deposited silver on the conductivity of silver-plated CF, four types of Ag/pCF with different silver weight percents were prepared, which were 25%, 35%, 45% and 55%, respectively. From the SEM images (Fig. 4), it could be seen that some Ag/pCF with 25% and 35% silver weight percent had defects in the silver layer and the size of the silver particles was not uniform, in which the Ag/pCF with 25% silver weight percent had more defects in the surface silver layer. With increasing silver weight percent, the silver layer was gradually perfected, the Ag/pCF with 45% silver weight percent had a uniform thickness of the surface silver layer with no defects, and the Ag/pCF with increased silver weight percent to 55% had an excessively thick surface silver layer, which was not uniform and showed a buildup of the silver particles. The results demonstrated that the Ag/pCF with 45% silver weight percent had formed a well-developed conductive network. Therefore, in the future work, we chose Ag/pCF with 45% silver weight percent for further study. The XRD results (Fig. 5a) show that the full width at half-maximum (FWHM) of the crys-

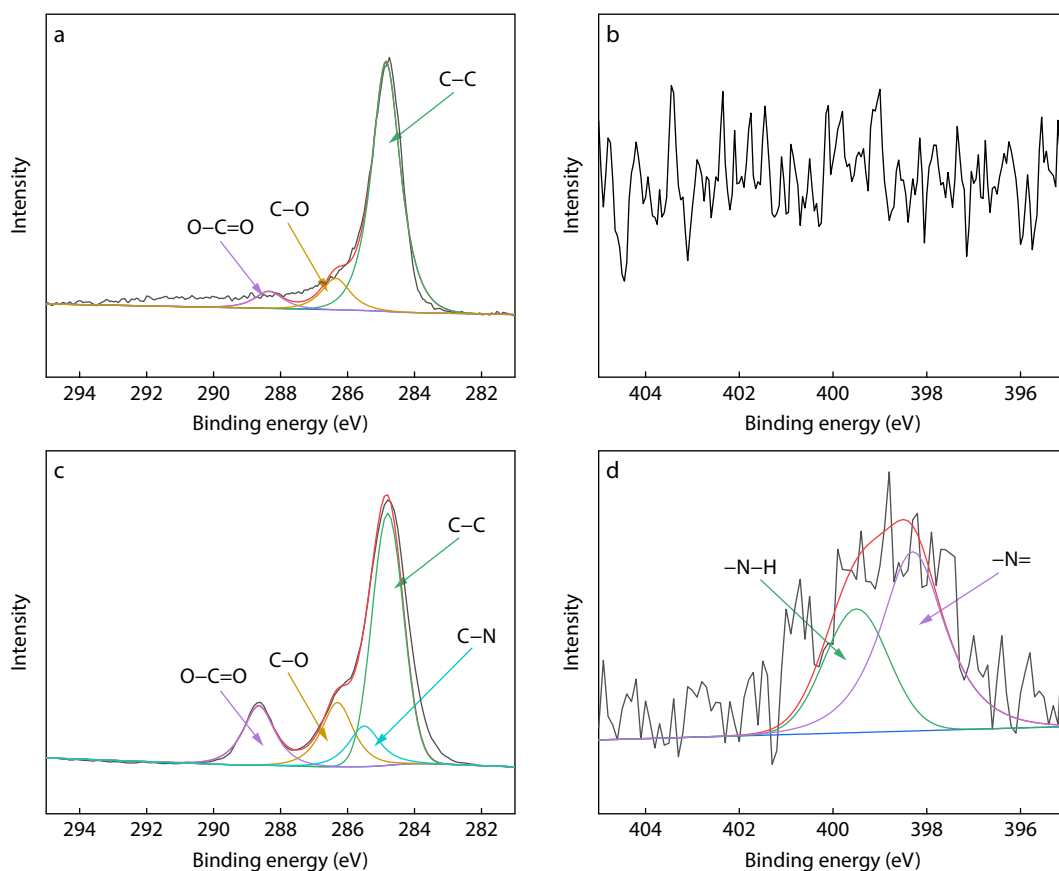


**Fig. 2** C 1s core-level spectra of neat CF (a) and pCF (c); N 1s core-level spectra of neat CF (b) and pCF (d).

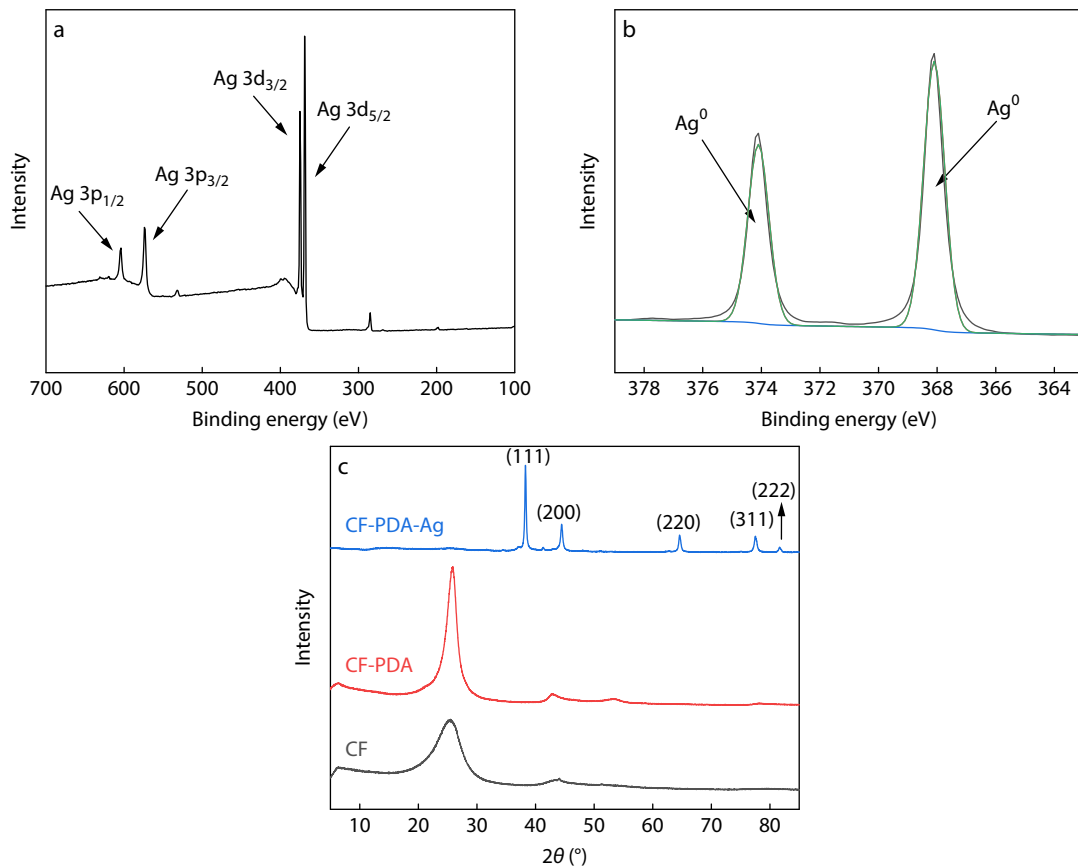


**Fig. 3** (a) XPS wide-scan and (b) Ag 3d spectra of Ag/pCF; XRD patterns of (c) Ag/pCF, pCF, and pristine CF.

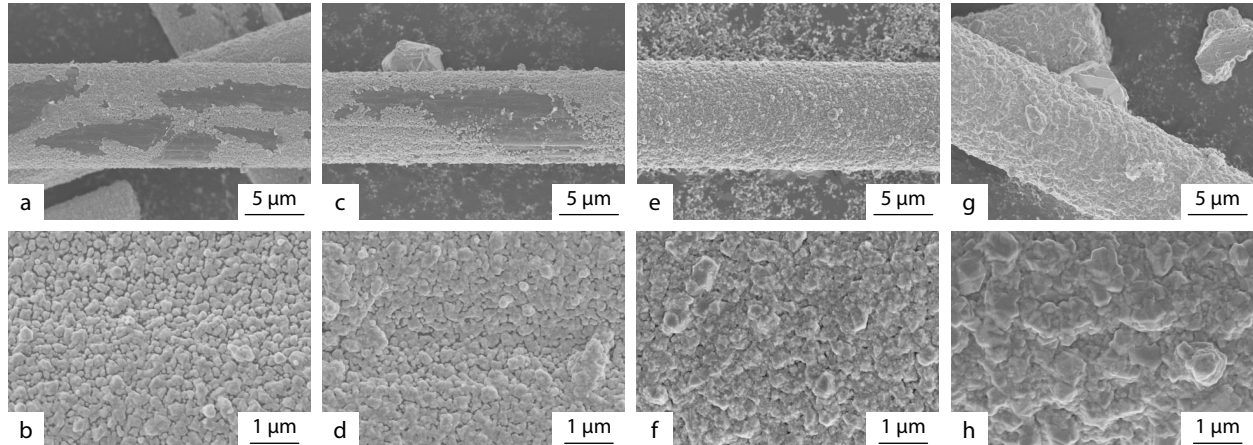


**Fig. 4** SEM images of Ag/pCF with different silver weight percents of (a, b) 25%, (c, d) 35%, (e, f) 45% and (g, h) 55%.

tal diffraction peaks of the silver layer becomes narrower, which indicated that the crystal defects of the silver layer were reduced, which was favorable for the movement of the free electrons, and the conductivity increased with the increase of the silver content (Fig. 5b).

The effect of reducing agents on the conductivity of Ag/pCF during electroless plating was explored, and the reducing agents were GLU, GLU:PSTT=1:1, PSTT, respectively. The silver particles in the silver layer on the Ag/pCF surface became smaller as the amount of PSTT in the reducing agent increased, the silver layer was smoother and denser, the dif-

fuse reflection of light on the surface was weaker, resulting in higher gloss, and the color of Ag/pCF is whiter and brighter (Figs. 6a–6c). The color of Ag/pCF is whiter and brighter. As shown in Fig. 7(a), the FWHM of the crystal diffraction peaks of the silver layer become narrower, indicating that the crystal defects of the silver layer were reduced, which was conducive to the movement of free electrons, the conductivity was also increased (Fig. 7b). The conductivity of Ag/pCF using PSTT as the reducing agent was 6392.5 S/cm, which was higher than the conductivity of Ag/pCF using GLU as the reducing agent (4471 S/cm), conductivity (4471 S/cm) by

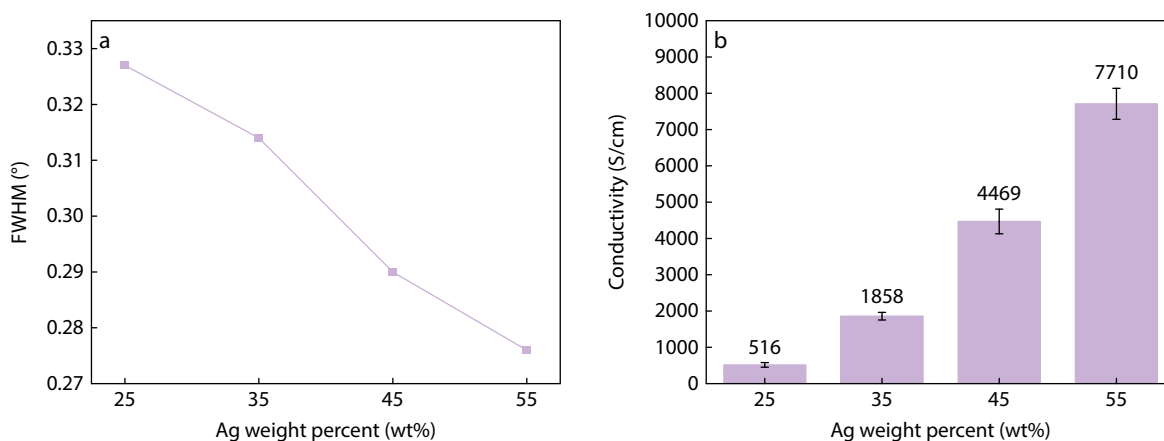


**Fig. 5** (a) Ag/pCF XRD peak FWHM changes with different silver weight percents; (b) Conductivity of Ag/pCF with different silver weight percents.

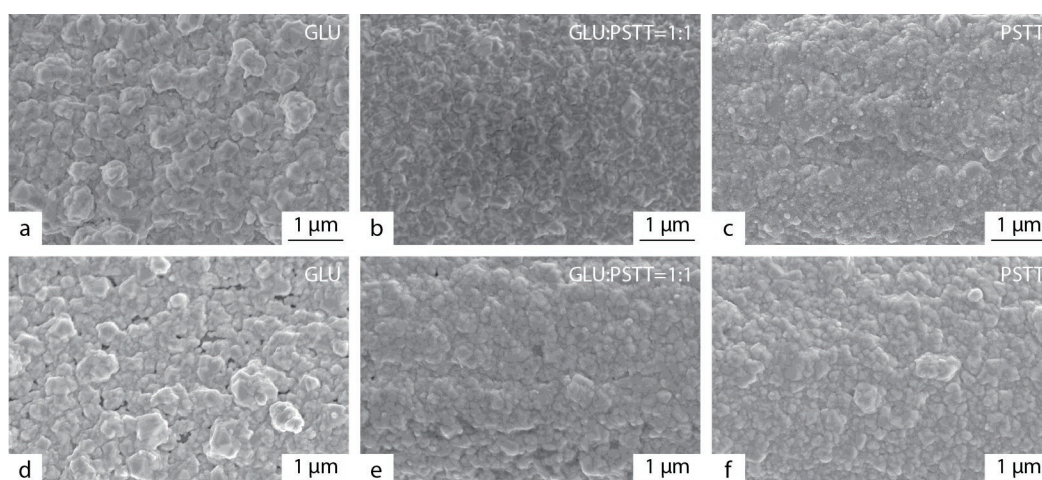


**Fig. 6** SEM images of Ag/pCF with different reducing agents before (a–c) and after (d–f) the salt spray corrosion simulation test.

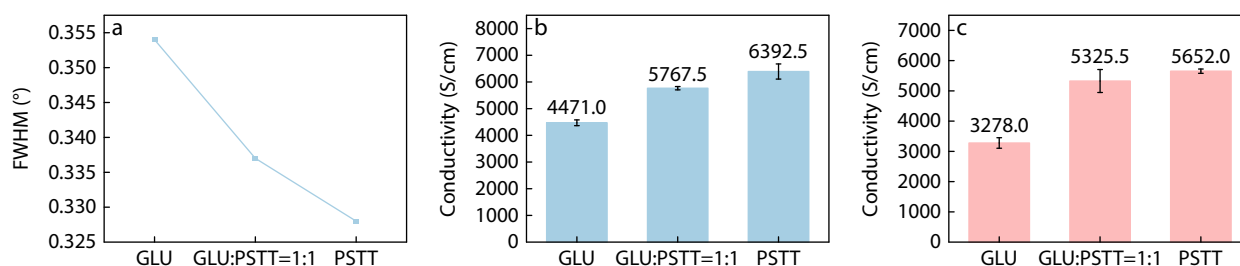


**Fig. 7** (a) Ag/pCF XRD peak FWHM changes with different reducing agents; Conductivity of Ag/pCF with different reducing agents before (b) and after (c) the salt spray erosion test.

42.97%. Ag/pCF was immersed in a solution containing 10% NaCl to simulate the erosion of salt spray on the particles. As shown in Fig. 7(c), after the salt spray simulation experiment, the conductivity of Ag/pCF using PSTT as the reducing agent layer was still the highest, probably due to the fact that the silver layer on the surface was denser and has fewer pores, so it was less subject to corrosion.

Ag/pCF was heat treated to further improved the conductivity of Ag/pCF. As shown in Fig. 8(a), the FWHM of the crystal diffraction peaks of the silver layer decrease after heat treatment, because the it was the process of melt recrystallization of the silver layer on the surface of Ag/pCF, and the

silver particles in the recrystallization process are more intact crystals, with fewer crystal lattice defects (*e.g.*, the appearance of vacancies, dislocations, and interstitial atoms), and the free electrons were subjected to a smaller resistance in the process of movement. As shown in Fig. 8(b), it can be seen that the conductivity of Ag/pCF increased after heat treatment, and the conductivity of Ag/pCF maintained at 200 °C for 90 min reached a maximum value of 7885 S/cm, which was 25.67% higher than that of untreated Ag/pCF (6274 S/cm). However, excessive heat treatment could lead to a decrease in conductivity, due to the fact that during annealing, molten silver tended to produce the smallest specific surface

area due to surface tension, which leads to the appearance of holes on the silver layer (Fig. 9), discontinuities in the silver layer, and consequently, a decrease in conductivity (Fig. 8b).

### Properties of Ag/pCF/MVQ Composites

Fig. 10 depicts the cross-sectional morphology of the Ag/pCF/MVQ composites. Ag/pCF was uniformly and disordered distributed in the silicone rubber, which was well bonded without any cavities observed. The silver layer on the surface of Ag/pCF did not come off even during the mixing and vulcanization process, which indicated that the CF was well bonded to the silver layer, which was attributed to the bonding effect of PDA.

The EMI SE of materials against electromagnetic waves can be broadly categorized into reflection shielding, absorption

shielding, and multiple reflection shielding, and the formulas are as follows:<sup>[43]</sup>

$$SE_T = SE_R + SE_A + SE_M \quad (1)$$

$$SE_R (\text{dB}) = -10 \lg(1 - R) \quad (2)$$

$$SE_A (\text{dB}) = -10 \lg \left( \frac{T}{1 - R} \right) \quad (3)$$

$$SE_T (\text{dB}) = -10 \lg T \quad (4)$$

Specifically,  $SE_M$  can be ignored when the  $SE_T$  of the material is  $>15$  dB. Quantitative analysis of the EMI SE of materials is often measured by vector network analyzers. It can present the incident and transmitted wave components in the form of

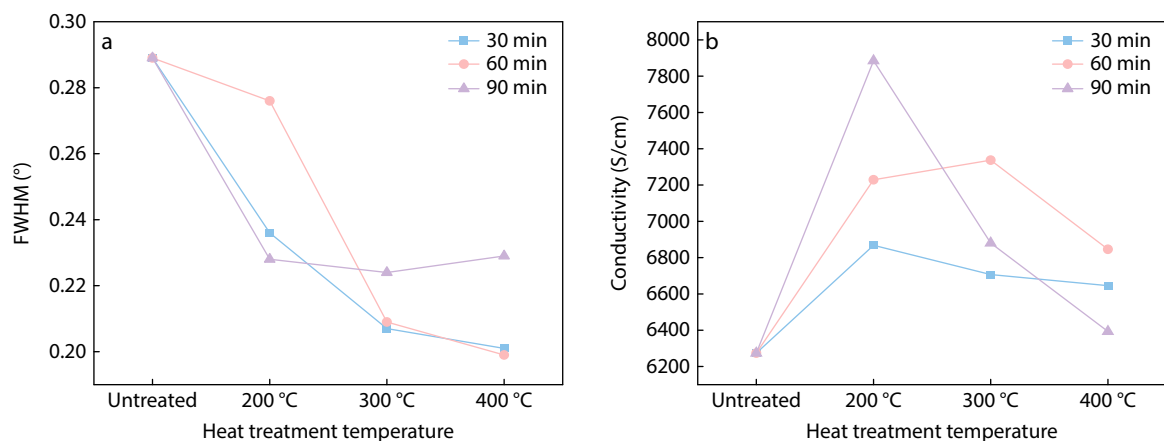


**Fig. 8** (a) Ag/pCF XRD peak FWHM changes after heat treatment; take the (111) peak as an example; (b) Conductivity of Ag/pCF after heat treatment.

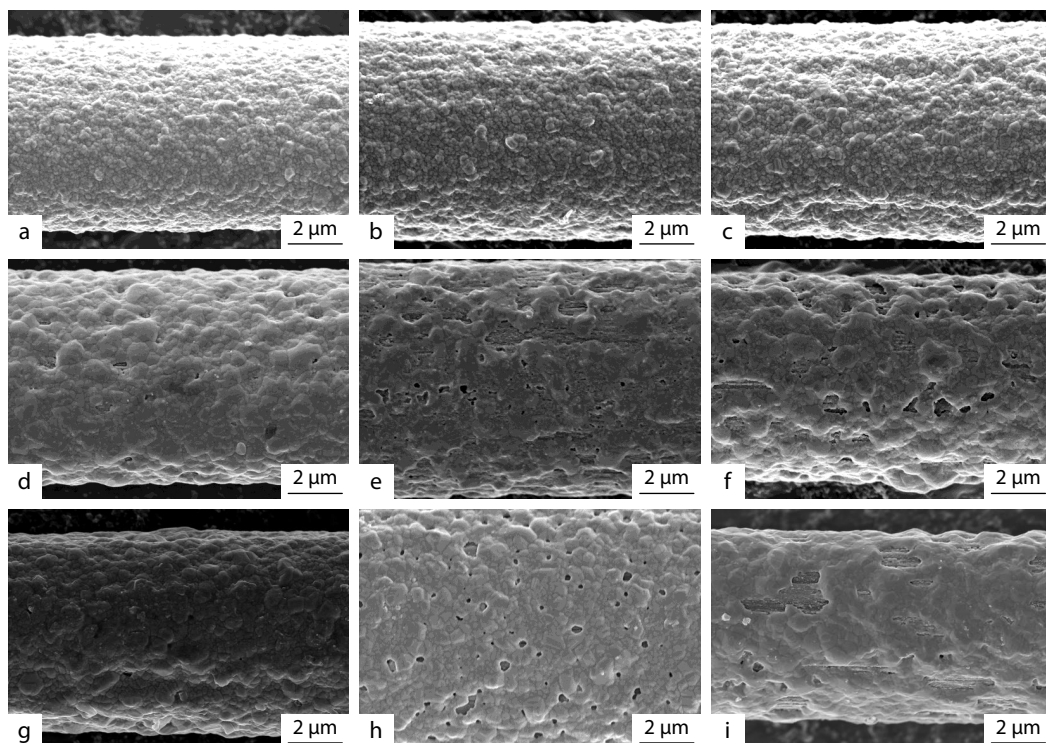


**Fig. 9** SEM images of Ag/pCF after heat treatment of (a) 200 °C × 30 min, (b) 200 °C × 60 min, (c) 200 °C × 90 min, (d) 300 °C × 30 min, (e) 300 °C × 60 min, (f) 300 °C × 90 min, (g) 400 °C × 30 min, (h) 400 °C × 60 min, (i) 400 °C × 90 min.

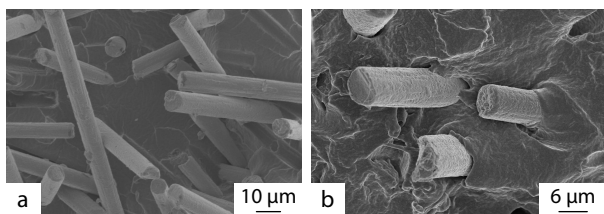


**Fig. 10** SEM images of Ag/pCF/MVQ composite.

S-parameters. The electromagnetic shielding mechanism of a material is usually analyzed by the absorption ( $A$ ), reflection ( $R$ ), and transmission coefficients ( $T$ ), which represent the proportion of electromagnetic waves absorbed, reflected, and transmitted, respectively, throughout the shielding material:

$$R = |S_{11}|^2, T = |S_{21}|^2, A = 1 - R - T \quad (5)$$

Fig. 11(a) depicts the shielding mechanism of the composite rubber. When the EM wave spread to the surface of the shielding material, because of the high impedance mismatch between the air and the material, most of the EM wave was reflected, a small amount of the EM wave was absorbed by the material and reflected many times inside the material, and the other part of the EM wave was absorbed by the composite rubber. In order to further explore the EMI shielding mechanism of the materials, five composite rubbers with different filler contents of 30, 35, 40, 45 and 50 phr were pre-

pared. With the increase of Ag/pCF filler content, Ag/pCF in the composite material began to contact each other and formed conductive pathways, and the conductivity and EMI SE increased, in which the EMI SE of the composite rubber with only 45 phr filler content in the X-band already exceeded 100 dB (Figs. 11b and 11c). As shown in Fig. 11(d), the reflected power coefficient ( $R$ ) was all greater than 0.8, and  $R$  of the composite rubber with a filler content of 45 phr was as high as 0.98 in the X-band. This indicated that 98% of the microwaves were reflected during the propagation process, only 2% of the microwaves were absorbed, and 99.99999999% of the microwaves were attenuated, indicated that the composite rubber was an EMI shielding material mainly for wave reflection.

The mechanical properties of Ag/pCF/MVQ composites are shown in Fig. 12. As a rigid inorganic fiber, the Shore hardness and density of the composites showed an increasing trend with the increase of Ag/pCF filler content. However, the increase in the filling content of Ag/pCF was not enhanced the mechanical properties of the composite rubber, which was due to the fact that the surface of Ag/pCF was chemically inert in general, and the lack of sufficient active groups led to the insufficient interaction between it and the rubber matrix, and the interface was easy to form a stress concentration point under the action of the external force, which negatively affected the mechanical properties of the material.

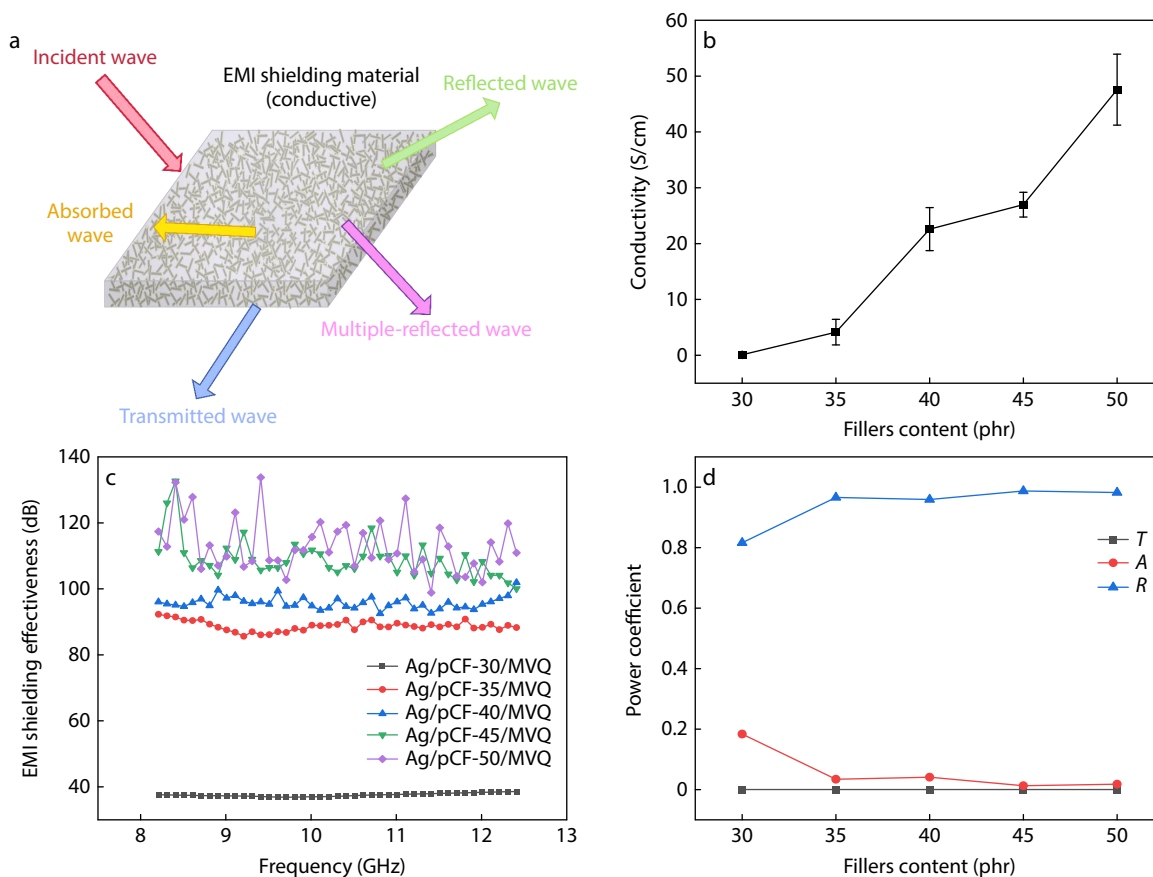


**Fig. 11** (a) Schematic diagram of EMI shielding mechanism for composite rubber; (b) Conductivity of composite rubber with different filler contents; (c) EMI shielding effectiveness of composite rubber; (d) Power coefficients of composite rubber.

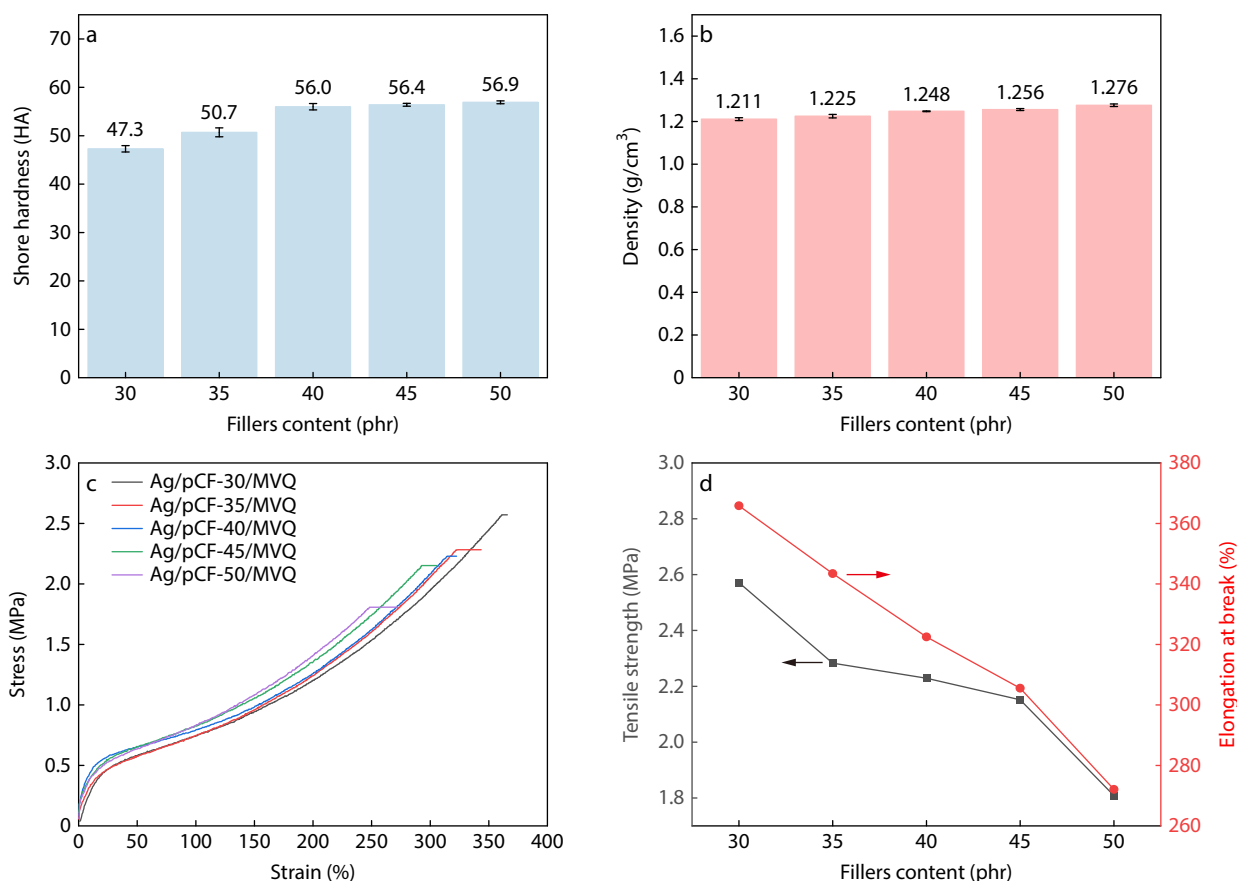


Fig. 12 Mechanical properties of the composite rubber.

## CONCLUSIONS

This work proposed a new method for composites to achieve high EMI SE at low filler fraction. Firstly, PDA was coated on the CF surface by oxidative self-polymerization. On this basis, silver layer was deposited on the CF surface by electroless silver plating. Finally, the composites were prepared by mechanical mixing method. The results showed that Ag/pCF with core-shell structure has a high electrical conductivity of 6274 S/cm and up to 7885 S/cm after heat treatment. The Ag/pCF/MVQ composite filled with 45 phr Ag/pCF possessed an excellent EMI SE of 111 dB with only 45 phr of filler. The composites could be used for EMI precision instruments, which provided a new method for the preparation of flexible, low-density and high EMI SE composites.

## Conflict of Interests

The authors declare no interest conflict.

## Data Availability Statement

Data requiring special software tools to open. The related data (DOI:10.57760/sciencedb.j00189.00041; CSTR:31253.11.sciencedb.j00189.00041) of this paper can be accessed in the Science Date Bank database <https://www.scidb.cn/s/rlzQ3>, and the

software for opening the data is Origin 2021.

## ACKNOWLEDGMENTS

This work was financially supported by the National Natural Science Foundation of China (No. 51833002).

## REFERENCES

- Kong, D.; Li, J.; Guo, A.; Xiao, X. High temperature electromagnetic shielding shape memory polymer composite. *Chem. Eng. J.* **2021**, *408*, 127365.
- Guo, H.; Chen, Y.; Li, Y.; Zhou, W.; Xu, W.; Pang, L.; Fan, X.; Jiang, S. Electrospun fibrous materials and their applications for electromagnetic interference shielding: a review. *Compos. Part A Appl. Sci. Manuf.* **2021**, *143*, 106309.
- Liu, J.; Yu, M. Y.; Yu, Z. Z.; Nicolosi, V. Design and advanced manufacturing of electromagnetic interference shielding materials. *Mater. Today Phys.* **2023**, *66*, 245–272.
- Cheng, J.; Li, C.; Xiong, Y.; Zhang, H.; Raza, H.; Ullah, S.; Wu, J.; Zheng, G.; Cao, Q.; Zhang, D.; Zheng, Q.; Che, R. Recent advances in design strategies and multifunctionality of flexible electromagnetic interference shielding materials. *Nanomicro. Lett.* **2022**, *14*, 80.
- Liang, C.; Gu, Z.; Zhang, Y.; Ma, Z.; Qiu, H.; Gu, J. Structural design strategies of polymer matrix composites for electromagnetic interference shielding: a review. *Nanomicro. Lett.* **2021**, *13*, 181.

- 6 Lee, S. H.; Yu, S.; Shahzad, F.; Hong, J.; Noh, S. J.; Kim, W. N.; Hong, S. M.; Koo, C. M. Low percolation 3D Cu and Ag shell network composites for EMI shielding and thermal conduction. *Compos. Sci. Technol.* **2019**, *182*, 107778.
- 7 Xie, Q.; Yan, Z.; Qin, F.; Wang, L.; Mei, L.; Zhang, Y.; Wang, Z.; Zhao, G.; Jiang, R. Metal carbide/Ni hybrids for high-performance electromagnetic absorption and absorption-based electromagnetic interference shielding. *Inorg. Chem. Front.* **2020**, *7*, 4832–4844.
- 8 Chen, X.; Liu, L.; Pan, F.; Mao, J.; Xu, X.; Yan, T. Microstructure, electromagnetic shielding effectiveness and mechanical properties of Mg-Zn-Cu-Zr alloys. *Mater. Sci. Eng. B-Adv.* **2015**, *197*, 67–74.
- 9 Wang, J. H.; Wu, R. Z.; Feng, J.; Zhang, J. H.; Hou, L. G.; Liu, M. D. Recent advances of electromagnetic interference shielding Mg matrix materials and their processings: a review. *T. Nonferr. Metal. Soc.* **2022**, *32*, 1385–1404.
- 10 Liang, C.; Liu, Y.; Ruan, Y.; Qiu, H.; Song, P.; Kong, J.; Zhang, H.; Gu, J. Multifunctional sponges with flexible motion sensing and outstanding thermal insulation for superior electromagnetic interference shielding. *Compos. Part A Appl. Sci. Manuf.* **2020**, *139*, 106143.
- 11 Wang, M.; Tang, X. H.; Cai, J. H.; Wu, H.; Shen, J. B.; Guo, S. Y. Fabrication, mechanisms and perspectives of conductive polymer composites with multiple interfaces for electromagnetic interference shielding: a review. *Carbon* **2021**, *177*, 377–402.
- 12 Yu, W. C.; Zhang, G. Q.; Liu, Y. H.; Xu, L.; Yan, D. X.; Huang, H. D.; Tang, J. H.; Xu, J. Z.; Li, Z. M. Selective electromagnetic interference shielding performance and superior mechanical strength of conductive polymer composites with oriented segregated conductive networks. *Chem. Eng. J.* **2019**, *373*, 556–564.
- 13 Zhang, J.; Wang, Q.; Xue, X.; Li, M.; Sun, X.; Zhao, J.; Zhang, W.; Lu, C. Waste flame-retardant polyurethane foam/ground tire rubber/carbon nanotubes composites with hierarchical segregated structures for high efficiency electromagnetic interference shielding. *Compos. Part A Appl. Sci. Manuf.* **2023**, *169*, 107530.
- 14 Feng, D.; Xu, D.; Wang, Q.; Liu, P. Highly stretchable electromagnetic interference (EMI) shielding segregated polyurethane/carbon nanotube composites fabricated by microwave selective sintering. *J. Mater. Chem. C* **2019**, *7*, 7938–7946.
- 15 Tudose, I. V.; Mouratis, K.; Ionescu, O. N.; Romanitan, C.; Pachiou, C.; Popescu, M.; Khomenko, V.; Butenko, O.; Chernysh, O.; Kenanakis, G.; Barsukov, V. Z.; Suche, M. P.; Koudoumas, E. Novel water-based paints for composite materials used in electromagnetic shielding applications. *Nanomaterials* **2022**, *12*, 487.
- 16 He, L.; Shao, X.; Tian, M.; Wang, W. Superhydrophobic and durable silver-coated fabrics for efficient electromagnetic interference shielding. *ACS Appl. Polym. Mater.* **2023**, *1*, 851–860.
- 17 Cheng, W.; Zhang, Y.; Tao, Y.; Lu, J.; Liu, J.; Wang, B.; Song, L.; Jie, G.; Hu, Y. Durable electromagnetic interference (EMI) shielding ramie fabric with excellent flame retardancy and Self-healing performance. *J. Colloid Interface Sci.* **2021**, *602*, 810–821.
- 18 Tugirumubano, A.; Vijay, S. J.; Go, S. H.; Kwac, L. K.; Kim, H. G. Characterization of electromagnetic interference shielding composed of carbon fibers reinforced plastics and metal wire mesh based composites. *J. Mater. Res. Technol.* **2019**, *8*, 167–172.
- 19 Xu, H.; Li, Y.; Han, X.; Cai, H.; Gao, F. Carbon black enhanced wood-plastic composites for high-performance electromagnetic interference shielding. *Mater. Lett.* **2021**, *285*, 129077.
- 20 Song, J.; Fan, Y.; Shi, A. Bidirectionally oriented carbon fiber/silicone rubber composites with a high thermal conductivity and enhanced electromagnetic interference shielding effectiveness. *Materials* **2023**, *16*, 6736.
- 21 Kruzelak, J.; Kvasnicakova, A.; Hlozekova, K.; Dosoudil, R.; Goralik, M.; Hudec, I. Electromagnetic interference shielding and physical-mechanical characteristics of rubber composites filled with manganese-zinc ferrite and carbon black. *Polymers* **2021**, *13*, 616.
- 22 Kruzelak, J.; Kvasnicakova, A.; Hlozekova, K.; Plavec, R.; Dosoudil, R.; Goralik, M.; Vilcakova, J.; Hudec, I. Mechanical, thermal, electrical characteristics and EMI absorption shielding effectiveness of rubber composites based on ferrite and carbon fillers. *Polymers* **2021**, *13*, 2937.
- 23 Fan, Z.; Guo, R.; Yang, Z.; Yang, Y.; Liu, X. The effect of the Co-blending process on the sensing characteristics of conductive chloroprene rubber/natural rubber composites. *Polymers* **2022**, *14*, 3326.
- 24 Zhang, H.; Zhang, G.; Gao, Q.; Zong, M.; Wang, M.; Qin, J. Electrically electromagnetic interference shielding microcellular composite foams with 3D hierarchical graphene-carbon nanotube hybrids. *Compos. Part A Appl. Sci. Manuf.* **2020**, *130*, 105773.
- 25 Zhang, C.; Lv, Q.; Liu, Y.; Wang, C.; Wang, Q.; Wei, H.; Liu, L.; Li, J.; Dong, H. Rational design and fabrication of lightweight porous polyimide composites containing polyaniline modified graphene oxide and multiwalled carbon nanotube hybrid fillers for heat-resistant electromagnetic interference shielding. *Polymer* **2021**, *224*, 123742.
- 26 Yang, H.; Yao, X.; Zheng, Z.; Gong, L.; Yuan, L.; Yuan, Y.; Liu, Y. Highly sensitive and stretchable graphene-silicone rubber composites for strain sensing. *Compos. Sci. Technol.* **2018**, *167*, 371–378.
- 27 Dou, Y.; Gu, H.; Sun, S.; Yao, W.; Guan, D. Synthesis of a grape-like conductive carbon black/Ag hybrid as the conductive filler for soft silicone rubber. *RSC Adv.* **2021**, *12*, 1184–1193.
- 28 Pazhooh, H. N.; Bagheri, R.; Adloo, A. Fabrication of semi-conductive natural rubber nanocomposites with low copper nanoparticle contents. *Polymer* **2017**, *108*, 135–145.
- 29 Luo, J. Q.; Zhao, S.; Zhang, H. B.; Deng, Z.; Li, L.; Yu, Z. Z. Flexible, stretchable and electrically conductive MXene/natural rubber nanocomposite films for efficient electromagnetic interference shielding. *Compos. Sci. Technol.* **2019**, *182*, 107754.
- 30 Ravindren, R.; Mondal, S.; Nath, K.; Das, N. C. Prediction of electrical conductivity, double percolation limit and electromagnetic interference shielding effectiveness of copper nanowire filled flexible polymer blend nanocomposites. *Compos. B Eng.* **2019**, *164*, 559–569.
- 31 Hao, M.; Li, L.; Shao, X.; Tian, M.; Zou, H.; Zhang, L.; Wang, W. Fabrication of highly conductive silver-coated aluminum microspheres based on poly(catechol/polyamine) surface modification. *Polymers* **2022**, *14*, 2727.
- 32 Shao, X.; Xu, W.; Yu, M.; He, L.; Hao, M.; Tian, M.; Wang, W. Improved salt spray resistance of silver-plated SiO<sub>2</sub> via self-assembled mercapto inhibitors. *ACS Appl. Polym. Mater.* **2023**, *1*, 1013–1023.
- 33 Yang, Y. H.; Pan, Y. X.; Feng, Z. H.; Shi, S. Evaluation of aerospace carbon fibers. *New Carbon Mater.* **2014**, *29*, 161–168.
- 34 Wei, J.; Liao, M.; Ma, A.; Chen, Y.; Duan, Z.; Hou, X.; Li, M.; Jiang, N.; Yu, J. Enhanced thermal conductivity of polydimethylsiloxane composites with carbon fiber. *Compos. Commun.* **2020**, *17*, 141–146.
- 35 Haghgoo, M.; Ansari, R.; Hassanzadeh-Aghdam, M. K.; Nankali, M. Analytical formulation for electrical conductivity and percolation threshold of epoxy multiscale nanocomposites reinforced with

- chopped carbon fibers and wavy carbon nanotubes considering tunneling resistivity. *Compos. Part A Appl. Sci. Manuf.* **2019**, *126*, 105616.
- 36 Qian, K.; Zhou, J.; Miao, M.; Wu, H.; Thaiboonrod, S.; Fang, J.; Feng, X. Highly ordered thermoplastic polyurethane/aramid nanofiber conductive foams modulated by kevlar polyanion for piezoresistive sensing and electromagnetic interference shielding. *Nanomicro. Lett.* **2023**, *15*, 88.
- 37 Qian, K.; Xu, Y.; Miao, M.; Deng, D.; Luo, L.; Feng, X. Engineering metalized surface of single hair via electroless Cu-plating strategy for self-supported nonenzymatic glucose sensor. *J. Mater. Sci.* **2023**, *58*, 15074–15085.
- 38 Ding, Y.; Weng, L.-T.; Yang, M.; Yang, Z.; Lu, X.; Huang, N.; Leng, Y. Insights into the aggregation/deposition and structure of a polydopamine film. *Langmuir* **2014**, *30*, 12258–12269.
- 39 Zhang, C.; Xiang, L.; Zhang, J.; Liu, C.; Wang, Z.; Zeng, H.; Xu, Z. K. Revisiting the adhesion mechanism of mussel-inspired chemistry. *Chem. Sci.* **2022**, *13*, 1698–1705.
- 40 Zhang, Z.; Si, T.; Liu, J.; Zhou, G. *In-situ* grown silver nanoparticles on nonwoven fabrics based on mussel-inspired polydopamine for highly sensitive sers carbaryl pesticides detection. *Nanomaterials* **2019**, *9*, 384.
- 41 Fu, Y.; Li, G.; Tian, M.; Wang, X.; Zhang, L.; Wang, W. Preparation of silver nanoparticle immobilized fibrillar silicate by poly(dopamine) surface functionalization. *J. Appl. Polym. Sci.* **2014**, *131*, 39859.
- 42 Wang, W.; Jiang, Y.; Wen, S.; Liu, L.; Zhang, L. Preparation and characterization of polystyrene/Ag core-shell microspheres—a bio-inspired poly(dopamine) approach. *J. Colloid Interface Sci.* **2012**, *368*, 241–249.
- 43 Jia, X.; Li, Y.; Shen, B.; Zheng, W. Evaluation, fabrication and dynamic performance regulation of green EMI-shielding materials with low reflectivity: a review. *Compos. B Eng.* **2022**, *233*, 109652.